# Supplementary Material

# Irregularly mechanical and thermal response of the N-H modes in the FOX-7 energetic material

Jushan Wang[1,2], Zhaoyang Zheng[2], Yangyang Zeng[2], Zanhao Wang[2], Guoyang Yu[2], Qi-Long Yan[3], Huashan Li[1]*, Yanqiang Yang[2]*, Biao Wang[1]

1) School of Physics, Sun Yat-sen University, Guangzhou 510275, China
2) National Key Laboratory of Shock Wave and Detonation Physics, Institute of Fluid Physics, China Academy of Engineering Physics, Mianyang 621900, China
3) National Key Laboratory of Solid Rocket Propulsion, Northwestern Polytechnical University, Xi'an 710072, China

**Experimental and calculation procedures**

The FOX-7 samples were synthesized by the Institute of Chemical Materials, China Academy of Engineering Physics. The ANDOR SR-500i Raman spectroscope is equipped with a triple polychromator and a liquid nitrogen-cooled charge-coupled device (CCD) detector. The 10x microscope objectives (Leica N PLAN series) were used for the high-pressure/temperature experiment. The entrance slit of the spectrometer was set to 10 μm. The sample was excited by a 532 nm line of an Ar ion laser. The laser power was set to 10 mW to avoid sample damage. The integral time of each spectrum was 10 seconds.

The Diamond Anvil Cell (DAC) furnished with a ruby stone chip about 10 μm diameter was used for pressure calibration. The pressure was calibrated by reference to the R1 fluorescence peak of the ruby. The sample had a relaxation time of 10 minutes at each pressure before the R1 line of ruby fluorescence was recorded. The pressures applied were measured using the ruby fluorescence method and the uncertainty of the measurement was within 0.02 GPa.

Given that FOX-7 energetic material is an organic compound, using a liquid pressure transfer medium (PTM), such as silicone oil or other organic substances, introduces challenges, including lower curing pressures and potential signal interference with the energetic material. Additionally, liquid pressure

media can influence the phase transition routes. In contrast, gas-based pressure transmission media exert a smaller effect on phase transitions but suffer from lower curing pressures, making them unsuitable for high-pressure phase transitions. To overcome these limitations, this study utilizes FOX-7 energetic material with particle sizes below 10 μm as the pressure transmission medium. Notably, no additional pressure transmission medium was used in the high-pressure experiments. For thermal detection, a Linkam stage (TS1500) was used. A platinum dish was used as a holder for the sample. The same powder sample was heated from room temperature to 453 K during the variable temperature measurements.

First-principles calculations were conducted using the plane-wave density-functional theory (DFT) as implemented in the Vienna Ab initio Simulation Package (VASP)[1, 2]. The Perdew-Burke-Ernzerhf (PBE) functional [3, 4] was adopted to describe the exchange-correlation potential. The core-valence interaction was described by the projected augmented waves (PAW) [5]. The electronic wave functions were expanded by plane wave basis with a kinetic energy cutoff of 800 eV. The Brillouin zone was sampled using a Monkhorst-Pack grid with a uniform separation of 0.03 $Å^{-1}$. The structural relaxations with and without pressure were carried out until the maximum force on each atom was less than 0.01 eV/Å. The Brillouin zone was sampled using a Monkhorst-Pack grid with a uniform separation of 0.03 $Å^{-1}$[6-8]. The projected augmented wave (PAW) method was utilized to describe the core-valence interactions between electrons. Geometry optimizations were performed until the maximum force on each atom was reduced to below 0.01 eV/Å. Hydrostatic pressure was incrementally increased by the steps of 0.5 GPa, starting from ambient pressure up to 10 GPa. It is noteworthy that the space group of the crystalline FOX-7 was constrained to remain unchanged throughout all geometry optimizations. Based on the optimized structures, the bond orders for solid nitromethane were also evaluated using density-derived electrostatic and chemical (DDEC) analysis[9]. The force constants and phonon spectra were calculated using the finite displacement method as implemented in PHONOPY package [10]. The crystal structures of α, α′ and ε-FOX-7 are derived from CCDC database with reference number 130779, and 2100143, respectively.

The geometric structure optimization and vibrational spectroscopy calculations were performed using the first-principles software CP2K based on density functional theory (DFT) (version v2025.1) for FOX 7 polymorphs[11]. The initial structures were derived from experimentally determined values[12, 13]. For α-FOX 7, the supercell was expanded to 2×2×1 (224 atoms); for β-FOX 7, a 2×2×1 supercell (224 atoms) was adopted; ε-FOX 7 utilized a 2×2×2 supercell (224 atoms); and γ-FOX 7 employed a 1×2×1

supercell (224 atoms). Geometric and cell optimizations were conducted separately for the four distinct crystalline phases. Calculations were performed using the Gaussian and augmented plane wave (GAPW) method for full-electron computations[14]. For the Gaussian basis set, the pob-TZVP-rev2 basis was employed[15], while the plane wave cutoff energy was set to 600 Ry. The exchange-correlation energy was described using the Perdew-Burke-Ernzerhof (PBE) functional[16], and dispersion interactions were corrected via Grimme's DFT-D3 dispersion correction with Becke-Johnson damping to account for higher-order many-body interactions[17, 18]. Convergence criteria for the cell optimization were as follows: maximum atomic displacement ≤ $1\times10^{-4}$ Bohr, root-mean-square displacement ≤ $5\times10^{-5}$ Bohr, maximum force ≤ $1\times10^{-5}$ Hartree/Bohr, and root-mean-square force ≤ $2\times10^{-5}$ Hartree/Bohr. The vibrational modes were obtained by diagonalizing the dynamical matrix following structural optimizations. The Raman activity of each mode was calculated using finite difference methods to compute the derivatives of the polarizability with respect to atomic displacements. This approach yielded the vibrational spectra and specific vibrational modes for each crystalline phase[19].

The variations in the Raman spectra of different crystalline phases of FOX-7 stem from the choice of functionals, basis sets, and van der Waals corrections, with the most significant contribution arising from anharmonic effects. The CRYSTAL package accounts for these effects through the Vibrational Self-Consistent Field method and fourth-order force constants, ensuring a more accurate description of vibrational properties.

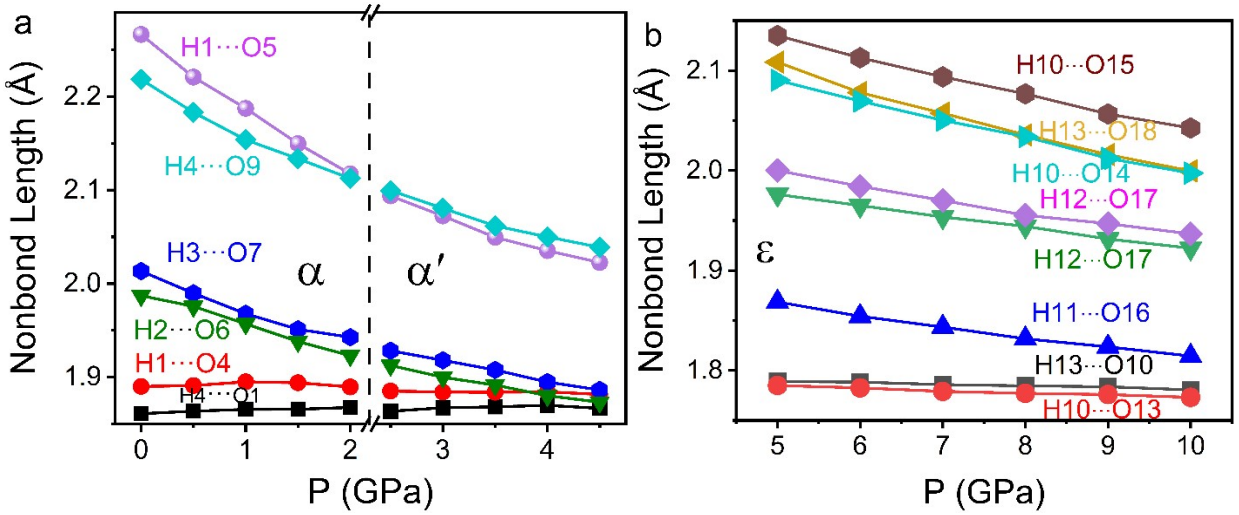

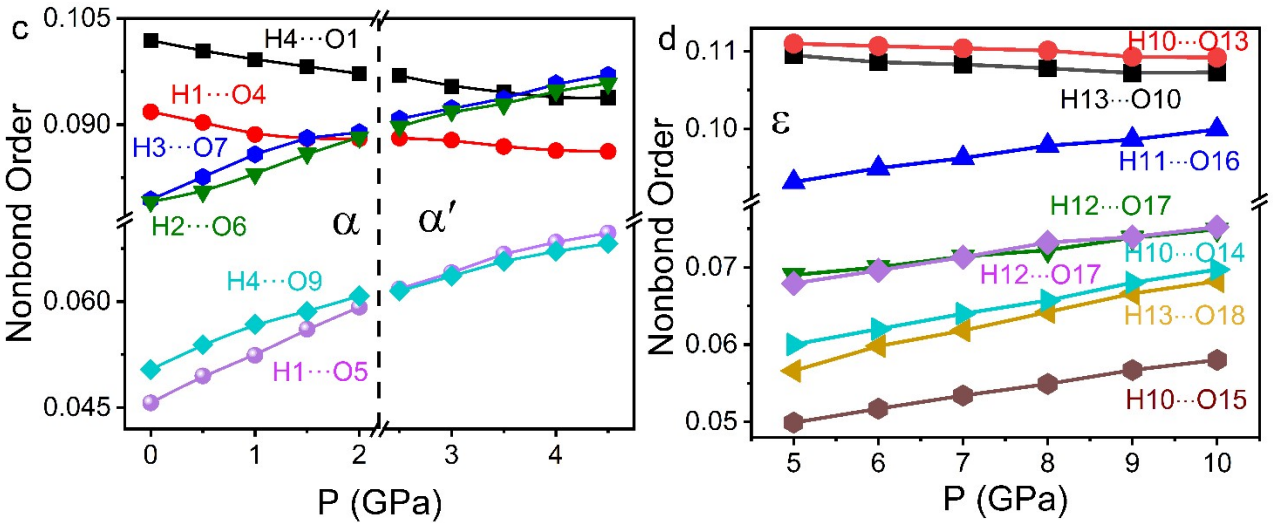


Figure S1 Compression derived relaxation of the (a, b) the H···O nonbonds length and (c, d) the H···O nonbonds order.

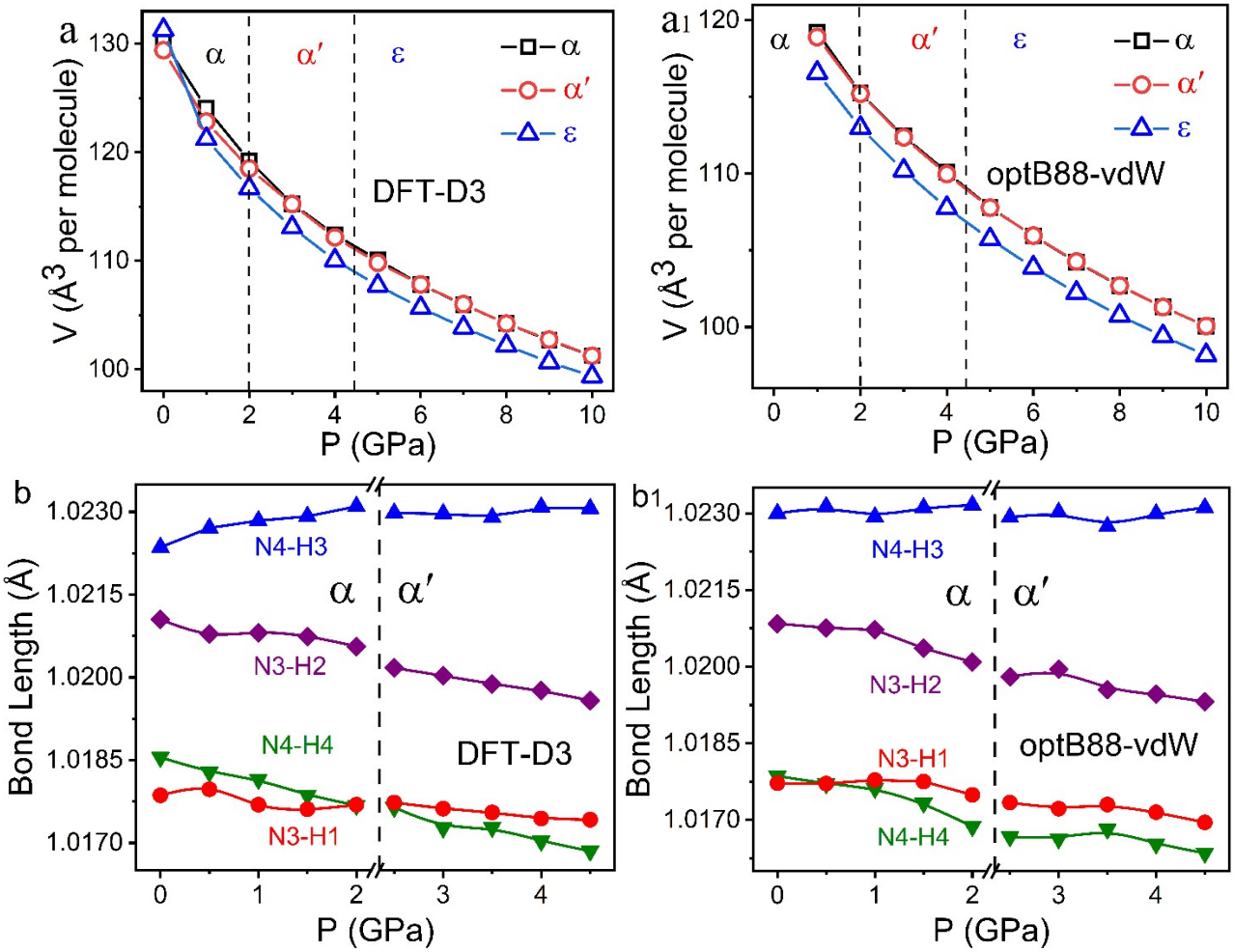

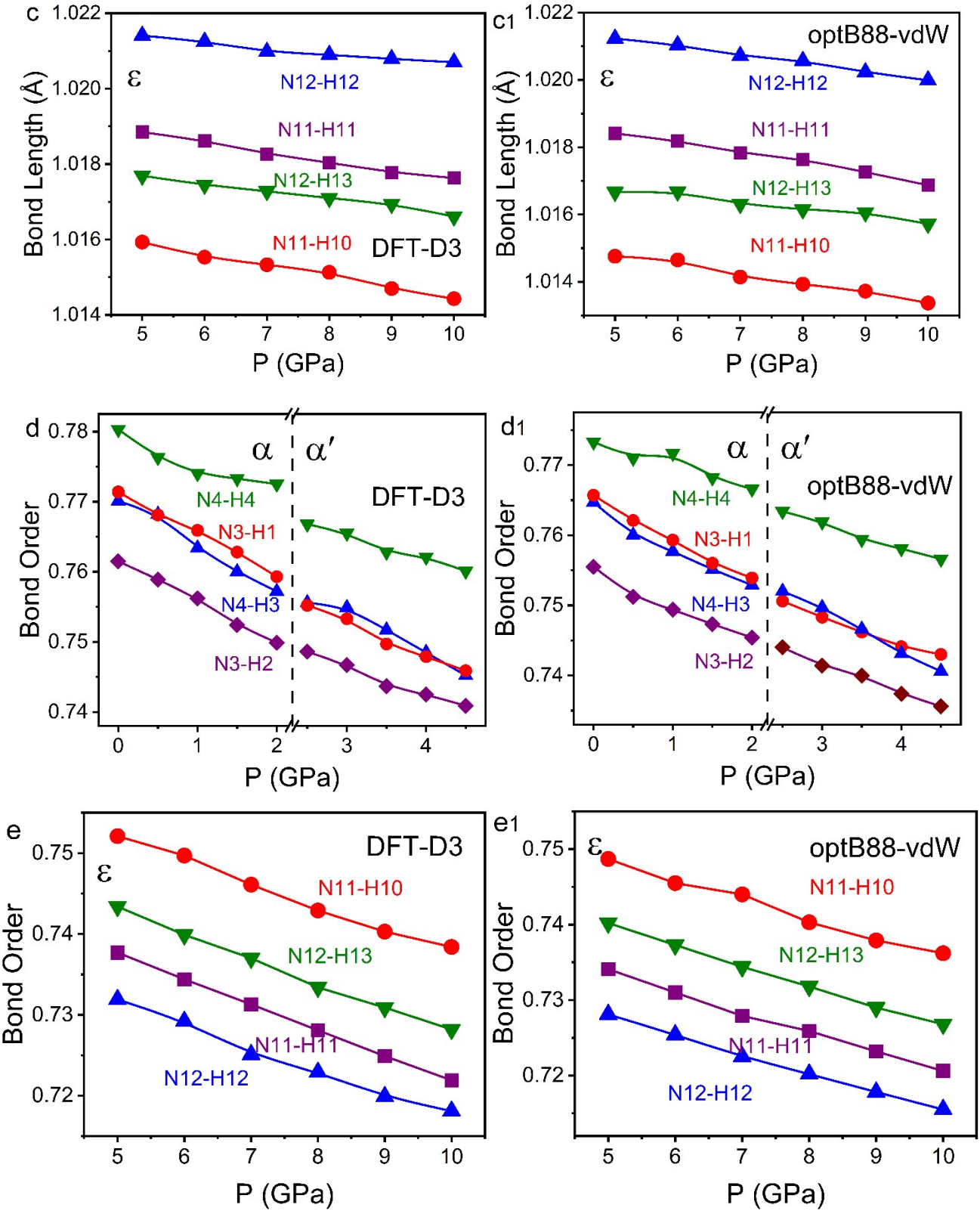
c
c1
d
d1
e
e1
Bond Length (Å)
Bond Order
P (GPa)
ε
α
α′
N12-H12
N11-H11
N12-H13
N11-H10
N4-H4
N3-H1
N4-H3
N3-H2
DFT-D3
optB88-vdW

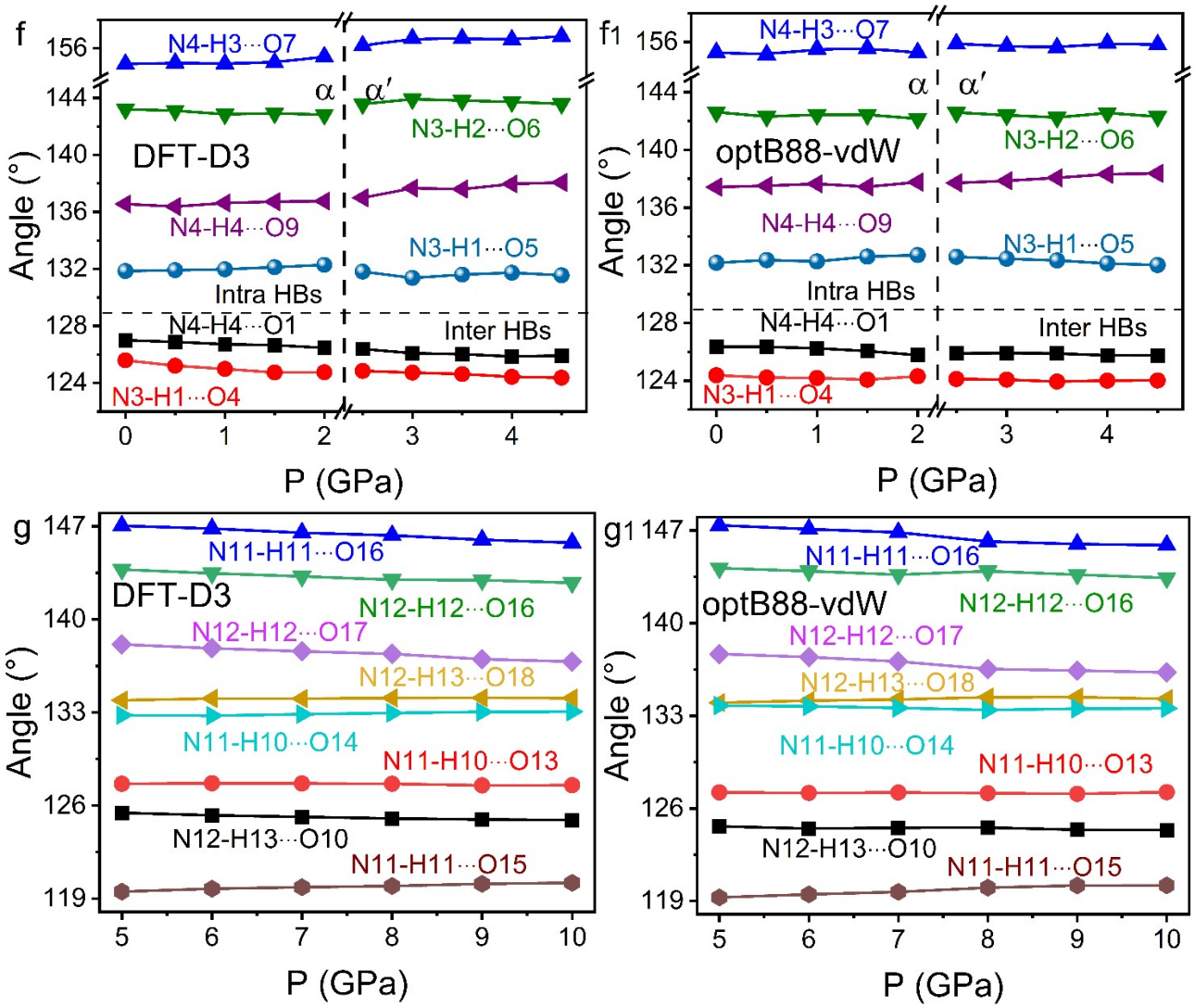


Figure S2. Comparison of volume, bond length, bond angle, and bond order of two computational methods (PBE-D3 and optB88-vdW) with changes in pressure.

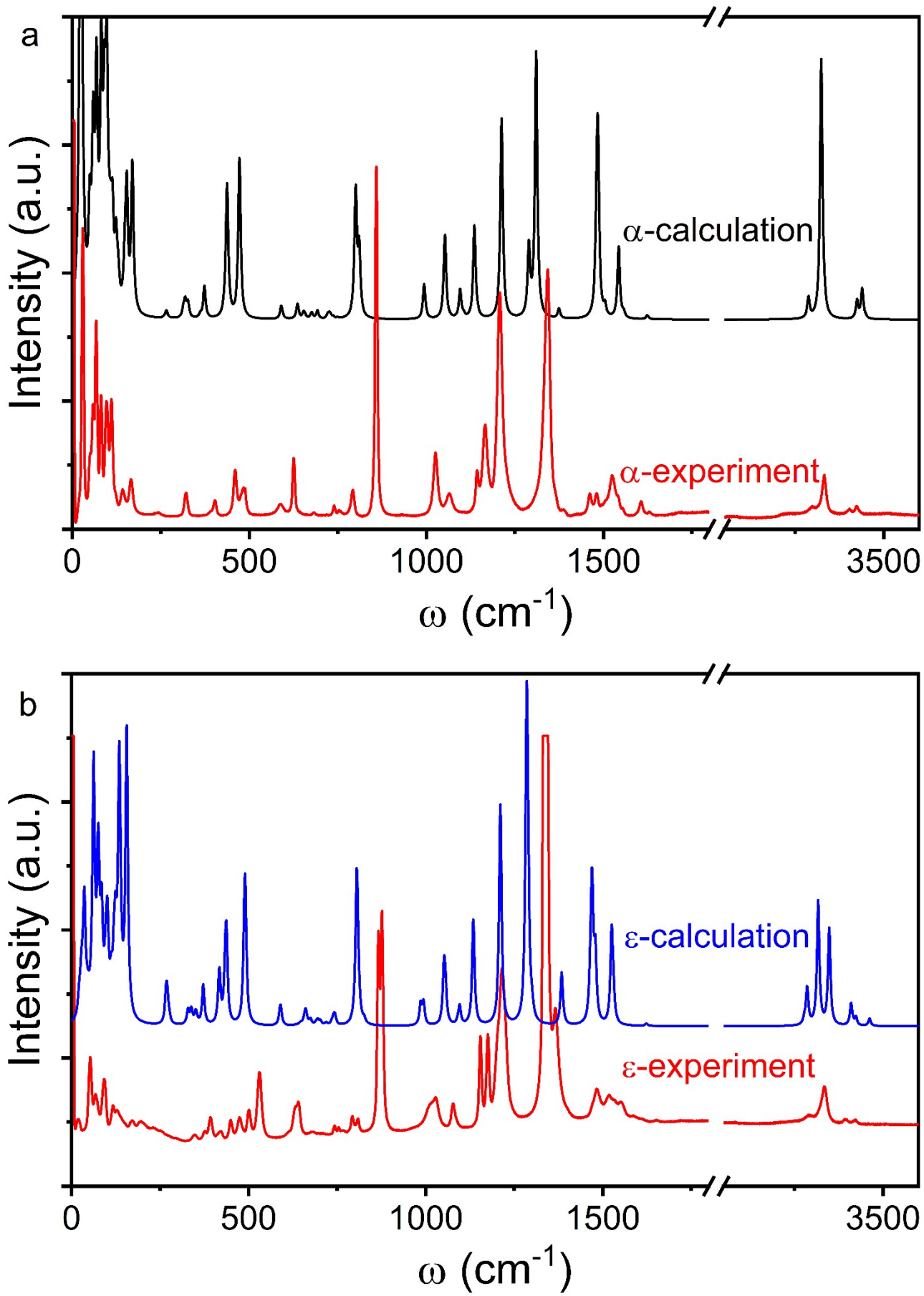
a
Intensity (a.u.)
α-calculation
α-experiment
0
500
1000
1500
3500
ω (cm-1)
b
Intensity (a.u.)
ε-calculation
ε-experiment
0
500
1000
1500
3500
ω (cm-1)

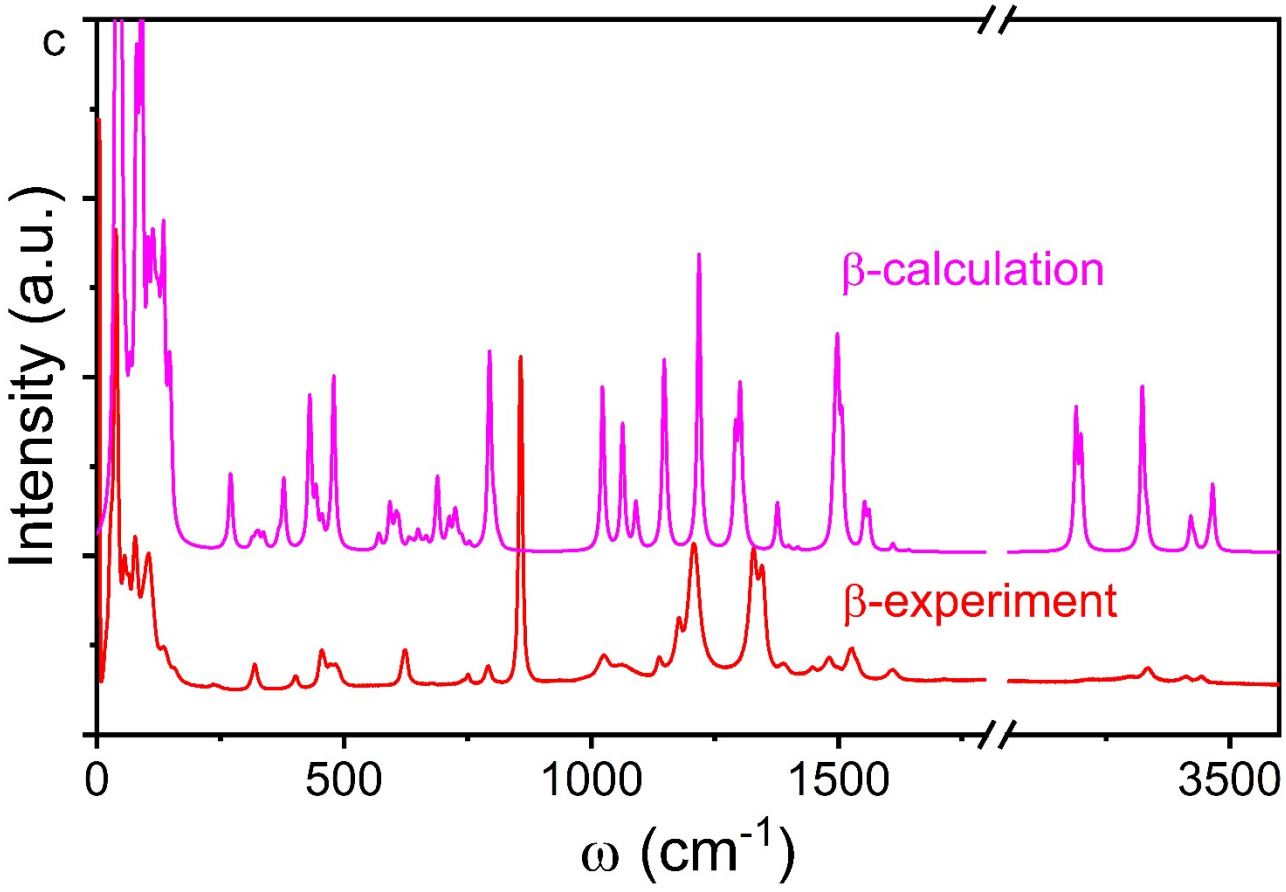
c
Intensity (a.u.)
β-calculation
β-experiment
0
500
1000
1500
3500
ω (cm-1)

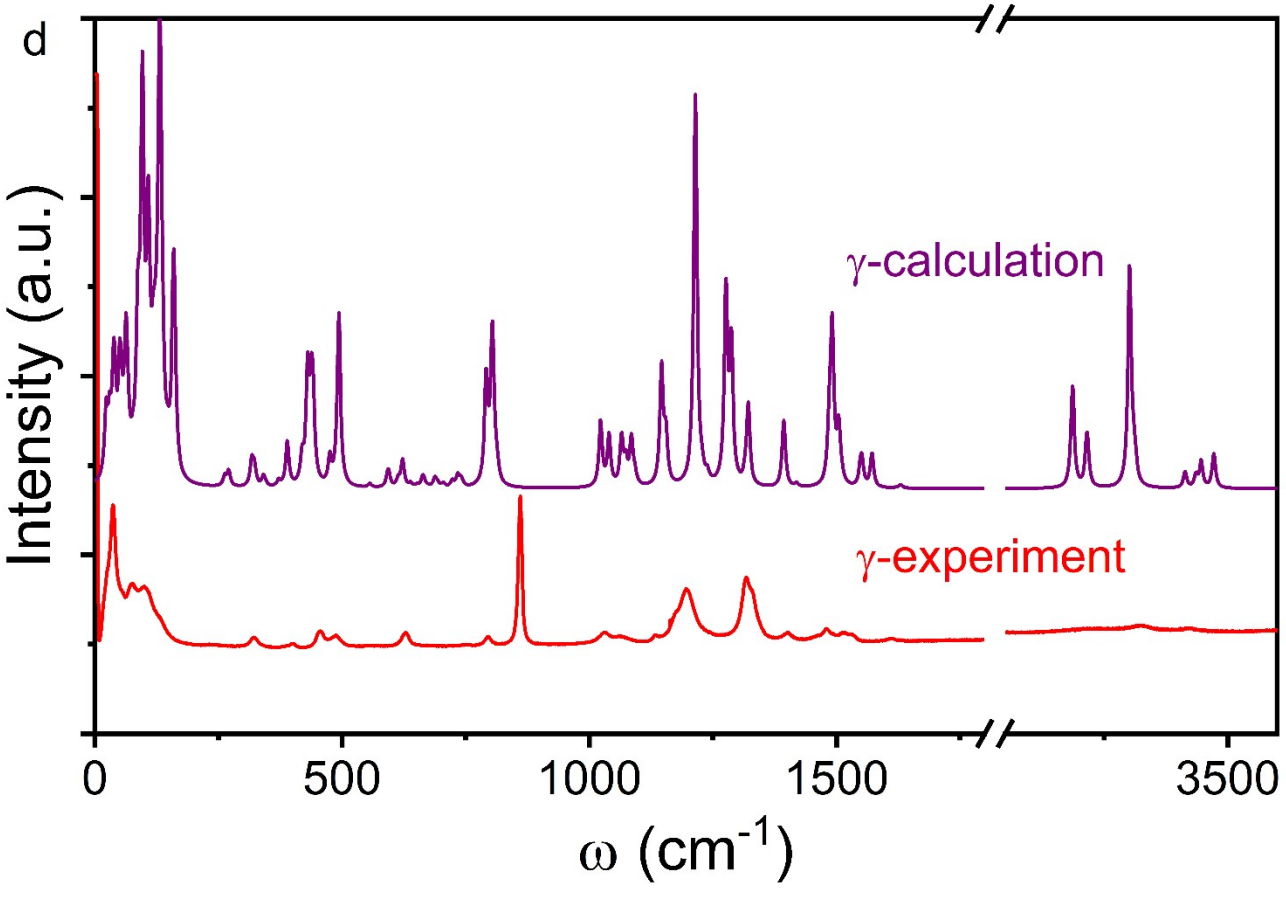
d
Intensity (a.u.)
γ-calculation
γ-experiment
0
500
1000
1500
3500
ω (cm-1)

Figure S3 Raman spectra calculated by DFT at 0K and experimentally tested by Raman spectrometer.

Table S1. Computationally and spectroscopically derived significant vibrational features for FOX-7 under the ambient pressure and temperature.

| Mode | Assignment | Raman frequency ($cm^{-1}$) | |
|---|---|---|---|
| | | this work | reference [13] |
| $\nu_{26}$ | $NH_2$ st. | 3424 | 3425 |
| $\nu_{25}$ | $NH_2$ st. | 3403 | 3405 |
| $\nu_{24}$ | $NH_2$ st. | 3332 | 3333 |
| $\nu_{23}$ | $NH_2$ st. | 3297 | 3299 |
| $\nu_{22}$ | $NH_2$ sci., C-$NH_2$ st. | 1632 | 1606 |
| $\nu_{21}$ | $NH_2$ b | 1606 | 1542 |
| $\nu_{20}$ | C-$NH_2$ sci. C-C st. | 1524 | 1528 |
| $\nu_{19}$ | C-C st. NH w | 1480 | 1506 |
| $\nu_{18}$ | C-C st. NH w | 1461 | 1464 |
| $\nu_{17}$ | C-$NO_2$ st. | 1387 | 1386 |
| $\nu_{16}$ | C-$NO_2$ st., NH w | 1343 | 1343 |
| $\nu_{15}$ | C-$NO_2$ st., NH w | 1208 | 1208 |
| $\nu_{14}$ | C-C st. NH w | 1167 | 1165 |
| $\nu_{13}$ | C-$NO_2$ st., NH w | 1143 | 1142 |
| $\nu_{12}$ | NH w | 1065 | 1070 |
| $\nu_{11}$ | NH w | 1026 | 1024 |
| $\nu_{10}$ | NH r | 859 | 856 |
| $\nu_9$ | C-$NO_2$ r | 793 | 789 |
| $\nu_8$ | NO w | 739 | 737 |
| $\nu_7$ | NH w | 684 | - |
| $\nu_6$ | NH w | 625 | 622 |
| $\nu_5$ | NH w and C-C st. | 588 | 583 |
| $\nu_4$ | $NH_2$ w, NO st. | 484 | 481 |
| $\nu_3$ | NH w | 460 | 457 |
| $\nu_2$ | NH w | 403 | 400 |
| $\nu_1$ | H w | 321 | 318 |
| $L_7$ | lattice vibration (non-bonding) | 166 | 162 |

| | | | |
|---|---|---|---|
| $L_6$ | lattice vibration (non-bonding) | 143 | 139 |
| $L_5$ | lattice vibration (non-bonding) | 111 | 107 |
| $L_4$ | lattice vibration (non-bonding) | 97 | 98 |
| $L_5$ | lattice vibration (non-bonding) | 81 | 77 |
| $L_4$ | lattice vibration (non-bonding) | 68 | 63 |
| $L_3$ | lattice vibration (non-bonding) | 59 | 54 |
| $L_2$ | lattice vibration (non-bonding) | 51 | 46 |
| $L_1$ | lattice vibration (non-bonding) | 30 | 25 |

Abbreviation: st: stretching, w: wagging, b: bending, r: rocking, sym: symmetric, asym: asymmetric.

Table S2. The vibration characteristics of N-H mode in FOX-7 through DFT calculation and experimental analysis.

| modes | Calculate Raman frequency ($cm^{-1}$) | Experimental Raman frequency ($cm^{-1}$) |
|---|---|---|
| N-H r | 800 | 859 |
| N-H w | 995 | 1026 |
| N-H st. | 3287 | 3297 |
| N-H st. | 3324 | 3332 |
| N-H st. | 3425 | 3403 |
| N-H st. | 3493 | 3424 |

## References


1. G. Kresse, J. Furthmuller, *Phys. Rev. B Condens Matter* (1996), **54**, 11169-11186.
2. M. L.Sun , J. P. Chou, J. F. Gao, Y. Cheng, A. Hu, W. C. Tang, Z. Gang, *ACS Omega* (2018), **3**, 8514-8520.
3. R. F. Zhang, D. Legut, Z. H. Fu, S. Veprek, Q. F. Zhang, H. K. Mao, *Phys. Rev. B* (2015), **92**, 1-6.
4. Z. Zheng, G. Yu, G. Zhu, Y. Yang, *Chem. Phys. Lett.* (2024), **837**.
5. M. Topsakal, R. M. Wentzcovitch, *Comp. Mater. Sci* (2014), **95**, 263-270.
6. B. Ghosh, S. Nahas, S. Bhowmick, A. Amit, *Phys. Rev. B* (2015), **91**, 115433.
7. B.-J. Wang, X.-H. Li, R. Zhao, X.-L. Cai, W.-Y. Yu, W.-B. Li, Z.-S. Liu, L.-W. Zhang, S.-H. Ke, *J. Mater. Chem. A* (2018), **6**, 8923-8929.
8. A. T. Nielsen, A. P. Chafin, S. L. Christian, D. W. Moore, M. P. Nadler, R. A. Nissan, D. J. Vanderah, R. D. Gilardi, C. F. George, J. L. Flippen-Anderson, *Tetrahedron* (1998), **54**, 11793-11812.
9. T. A. Manz, *RSC Adv.* (2017), **7**, 45552-45581.

10. A. Togo, I. Tanaka, *Scripta. Mater* (2015), **108**, 1-5.

11. T. D. Kuhne, M. Iannuzzi, M. Del Ben, V. V. Rybkin, P. Seewald, F. Stein, T. Laino, R. Z. Khaliullin, O. Schutt, F. Schiffmann, D. Golze, J. Wilhelm, S. Chulkov, M. H. Bani-Hashemian, V. Weber, U. Borstnik, M. Taillefumier, A. S. Jakobovits, A. Lazzaro, H. Pabst, T. Muller, R. Schade, M. Guidon, S. Andermatt, N. Holmberg, G. K. Schenter, A. Hehn, A. Bussy, F. Belleflamme, G. Tabacchi, A. Gloss, M. Lass, I. Bethune, C. J. Mundy, C. Plessl, M. Watkins, J. VandeVondele, M. Krack, J. Hutter, *J. Chem. Phys.* (2020), **152**, 194103.

12. Zbigniew A. Dreger, Y. M. Gupta, *J. Phys. Chem. A* (2010), **114**, 7038-7047.

13. Z. A. Dreger, Y. Tao, Y. M. Gupta, *J. Phys. Chem. A* (2014), **118**, 5002-5012.

14. J. H. Gerald Lippert, Michele Parrinello, *Theo. Chem. Acc.* (1999), **103**, 124-140.

15. D. Vilela Oliveira, J. Laun, M. F. Peintinger, T. Bredow, *J. Comput. Chem.* (2019), **40**, 2364-2376.

16. K. B. John P. Perdew, Matthias Ernzerhof, *Phys. Rev. Lett.* (1996), **77**, 3865-3868.

17. S. Grimme, S. Ehrlich, L. Goerigk, *J. Comput. Chem.* (2011), **32**, 1456-65.

18. S. Grimme, J. Antony, S. Ehrlich, H. Krieg, *J Chem Phys* (2010), **132**, 154104.

19. A. Putrino, D. Sebastiani, M. Parrinello, *J. Chem. Phys.* (2000), **113**, 7102-7109.